Earthquakes and Structures, *Vol. 8, No. 3 (2015) 555-572*
DOI: http://dx.doi.org/10.12989/eas.2015.8.3.555

Seismic behavior of steel reinforced concrete (SRC) T-shaped column-beam planar and 3D hybrid joints under cyclic loads

Zongping Chen[1,2a], Jinjun Xu[*1], Yuliang Chen[1] and Jianyang Xue[1b]

[1]*College of Civil Engineering and Architecture, Guangxi University, Guangxi, China*
[2]*Key Laboratory of Disaster Prevention and Structural Safety of Chinese Education Ministry, Guangxi, China*

(Received February 14, 2014, Revised May 27, 2014, Accepted June 21, 2014)

Abstract. This paper presents an experimental study of three two-dimensional (2D/planar) steel reinforced concrete (SRC) T-shaped column-RC beam hybrid joints and six 3D SRC T-shaped column-steel beam hybrid joints under low cyclic reversed loads. Considering different categories of steel configuration types in column cross section and horizontal loading angles for the specimens were selected, and a reliable structural testing system for the spatial loading was employed in the tests. The load-displacement curves, carrying capacity, energy dissipation capacity, ductility and deformation characteristics of the test subassemblies were analyzed. Especially, the seismic performance discrepancies between planar hybrid joints and 3D hybrid joints were intensively compared. The failure modes for planar loading and spatial loading observed in the tests showed that the shear-diagonal compressive failure was the dominating failure mode for all the specimens. In addition, the 3D hybrid joints illustrated plumper hysteretic loops for the columns configured with solid-web steel, but a little more pinched hysteretic loops for the columns configured with T-shaped steel or channel-shaped steel, better energy dissipation capacity & ductility, and larger interlayer deformation capacity than those of the planar hybrid joints. Furthermore, it was revealed that the hysteretic loops for the specimens under 45° loading angle are generally plumper than those for the specimens under 30° loading angle. Finally, the effects of steel configuration type and loading angle on the seismic damage for the specimens were analyzed by means of the Park-Ang model.

Keywords: steel reinforced concrete (SRC); T-shaped column; hybrid joint; planar joint; 3D joint; seismic behavior; loading angle; damage

1. Introduction

Special shaped column is a column with L-shaped, T-shaped, +-shaped or Z-shaped cross sections, which is located in the corner of frame structures, and its advantage is saving the indoor space and convenient for the furniture arrangement (Zhou *et al*. 2012, Wu *et al*. 2009, Xu *et al*. 2009, Patton *et al*. 2012). In past decades, the reinforced concrete (RC) special shaped columns have been extensively studied. Ramamurthyhe *et al*. (1983), Marin (1979) Cheng-Tzu (1985) and Hsu (1989) provided the methods of calculating the static performance of RC L-shaped columns,

∗Corresponding author, Ph.D. Candidate, E-mail: jjxu_concrete@163.com; zpchen@gxu.edu.cn
[a]Professor, E-mail: zpchen@gxu.edu.cn
[b]Professor

http://www.techno-press.org/?journal=eas&subpage=7 ISSN: 2092-7614 (Print), 2092-7622 (Online)

including the ultimate bearing capacity, the load-bending moment curve and the relationship between bending moment and curvature. From 1990's to the beginning of 2000's, many scholars such as Mallikarjuna *et al.* (1992), Tsao *et al*. (1993), Dundar *et al*. (1993), Yau *et al*. (1993), Sinha (1996) started to make computer programs for different kinds of special shaped columns to calculate their bearing capacities under bi-axial eccentric compression. Several researchers, such as Kang *et al*. (1997), Li *et al*. (2002), Zhao *et al*. (2004), Cao *et al*. (2005) carried out experimental investigations to reveal the seismic behavior of RC special shaped columns under low cyclic reversed loading, and all the test results indicated that the main seismic indexes of RC special shaped columns were inferior to those of RC rectangle columns.

Up to now, with the development of structural system, steel-concrete (SC) composite structures start to show their stronger performance and better economic advantages compared with RC structures. Due to the limitation of RC materials (e.g., bearing capacity and deformability), two types of SC special shaped columns, such as steel reinforced concrete (SRC) special shaped columns and concrete filled steel tube (CFST) special shaped columns, were proposed by Xue *et al*. (2012), Zuo *et al*. (2012), respectively. Later, Wang *et al*. (2013) carried out a numerical study of axially loaded T-shaped CFST columns via ABAQUS analysis, and then proposed a simplified formulae for designing calculation. In addition, considerable works were carried out to describe the behavior of eccentrically loaded the steel fibre high strength RC columns. Therefore, based on the before-mentioned ideas, Tokgoz *et al*. (2012) developed a new kind of SC composite special shaped column called L-shaped steel fibre high strength RC composite columns to test their biaxial bending performance and the behavior under short-term axial compression.

As more recently been recognized, the earthquake damage identification has been a new development direction in the seismic resistant design of structures. To guarantee the normal work of a structure, it is a basis that to meet the security and reliability for beam-column joint. On the basis of these concepts, several experimental and numerical studies have been conducted in recent years. Li and Kulkarni (2010) carried out an experimental and numerical investigation on RC wide beam-column joints when subjected to seismic loads. The efficiency of using fiber-reinforced polymer (FRP) strengthening RC interior beam-column joints, which had been tested under constant axial compression load and reversed cyclic loading, was investigated by Li and Chua (2009). The performance of exterior and interior beam-column subassemblages following the loss of one of the ground exterior columns was experimentally studied by Yap and Li (2011) and Kai and Li (2012), respectively.

As a mater of fact, the actual horizontal seismic action is in a state of multidimensional, therefore, it is essential to evaluate the effect of multi-directional loading on the seismic performance of a structure to develop more reliable design procedures. Pham and Li (2013) conducted an experimental and numerical investigation on RC columns with light transverse reinforcement with an emphasis on how varying the directions of seismic loading influences the seismic failure mechanisms of the columns. Due to the effect of horizontal loads, the joints in beam-column frame structures are generally in the state of multi-axis complex stress, including the axial force, shear force, bending moment and even torque, so that they can become a weak link for the seismic design of a frame structure. In spite of the extensive studies of SRC/RC rectangular column-RC/steel beam hybrid joints in the literature, the topics on the seismic behavior of SRC special shaped column-beam two-dimensional (2D/planar) and three-dimensional (3D) hybrid joints still have not been fully addressed.

In this paper, low cyclic reversed loading tests on three SRC T-shaped column-RC beam planar joints and six SRC T-shaped column-steel beam 3D joints were firstly conducted to investigate

their seismic behaviors. Then, the load-displacement hysteretic relationships, failure modes, energy dissipation capacity, ductility and deformation characteristics of all the specimens was discussed. Especially, the seismic performances between the planar joint and the 3D joint were compared in detail. In addition, the effects of steel configuration type and horizontal loading angle on the seismic damage for the specimens were analyzed by means of the Park-Ang model.

2. Experimental program

2.1 Specimen characteristics

2.1.1 2D/planar joints

In this investigation, assuming that the positions of inflection points are determined from the results of the global structural analysis, a tee-shaped subassembly along with the boundary and loading conditions can simulate parts of a structure subjected to the horizontal seismic-induced moment. Hence, three SRC T-shaped column-RC beam planar hybrid joints located at the middle storey of a frame structure were selected for the scale model tests. In considerations of the available maximum loading capacity of the actuator and the conditions of the laboratory, the scale ratio of the specimens was finally determined as 1:2. The detailed dimensions of the 2D specimens are shown in Fig. 1 and Table 1. The test parameters such as steel configuration type in column cross section, axial compression ratio (n) and ratio of column limb height to thickness were considered to study the seismic behavior of 2D hybrid joints.

The distance of the upper column end (named upper inflection point) to the bottom column end (named nether inflection point) is 1637.5 mm, and the distance of inflection point of the concrete beam to the T-shaped column limb end is 1100 mm. As for the concrete strength of planar hybrid joints, their average cubic compressive strength f_{cu} (the length of the standard cubic concrete sample is 150 mm) obtained on the same time of testing the specimens are 43.67 MPa.

2.1.2 3D joints

Considering the spatiality, six SRC T-shaped column-steel beam 3D hybrid joints were

Table 1 Characteristics of the column-beam joint specimens

Specimen code	Shape steel form	θ(°)	n	Ratio of column limb height to thickness	Longitudinal shape steel ratio (%)	Longitudinal steel reinforcement ratio (%)
PTJ1	T-shaped steel	0	0.28	3.0	3.60	0.22
PTJ2	Channel-shaped steel	0	0.30	4.0	4.34	0
PTJ3	Solid-web steel	0	0.29	2.0	5.45	0.52
STJ1	Channel-shaped steel	30	0.30	3.4	4.78	0
STJ2	Solid-web steel	30	0.30	3.4	4.90	0.39
STJ3	T-shaped steel	30	0.30	3.4	4.26	0.39
STJ4	T-shaped steel	45	0.30	3.4	4.26	0.39
STJ5	Channel-shaped steel	45	0.30	3.4	4.78	0
STJ6	Solid-web steel	45	0.30	3.4	4.90	0.39

designed from the model of a 3D frame structure. In considerations of the available maximum loading capacity of the actuator and the conditions of the laboratory, the scale ratio of the specimens was finally determined as 1:2. The detailed dimensions of the 3D specimens are shown in Fig. 2 and Table 1, where the cross section sizes and the lengths of all the H-type steel beams welded in 3D hybrid joints are kept the same. The test parameters such as steel configuration type in column cross section and loading angle (θ) were considered to study the seismic behavior of 3D hybrid joints.

The distance of the upper column end to the bottom column end is 1600 mm, and the distances of inflection points of all the steel beams to the T-shaped column limb ends are 900 mm. In order to investigate the spatial mechanical behavior of 3D joint, the earthquake directions to the structure were considered in the test, and these action directions shown in Fig. 3 were designed in the form of lateral loading angles (θ=30° and 45°). As for the concrete strength of 3D hybrid joints, their average cubic compressive strength f_{cu} obtained on the same time of testing the specimens are 29.67 MPa.

2.2 Fabrication of shape steels

As illustrated in Fig. 1 and Fig. 2, three types of shape steels in T-shaped cross section for the column are configured, including the channel-shaped steel, T-shaped steel and solid-web steel. The channel-shaped steel and T-shaped steel were connected through the horizontal steel flats welded, and all the steel beams for 3D hybrid joints were also welded to the steel flanges.

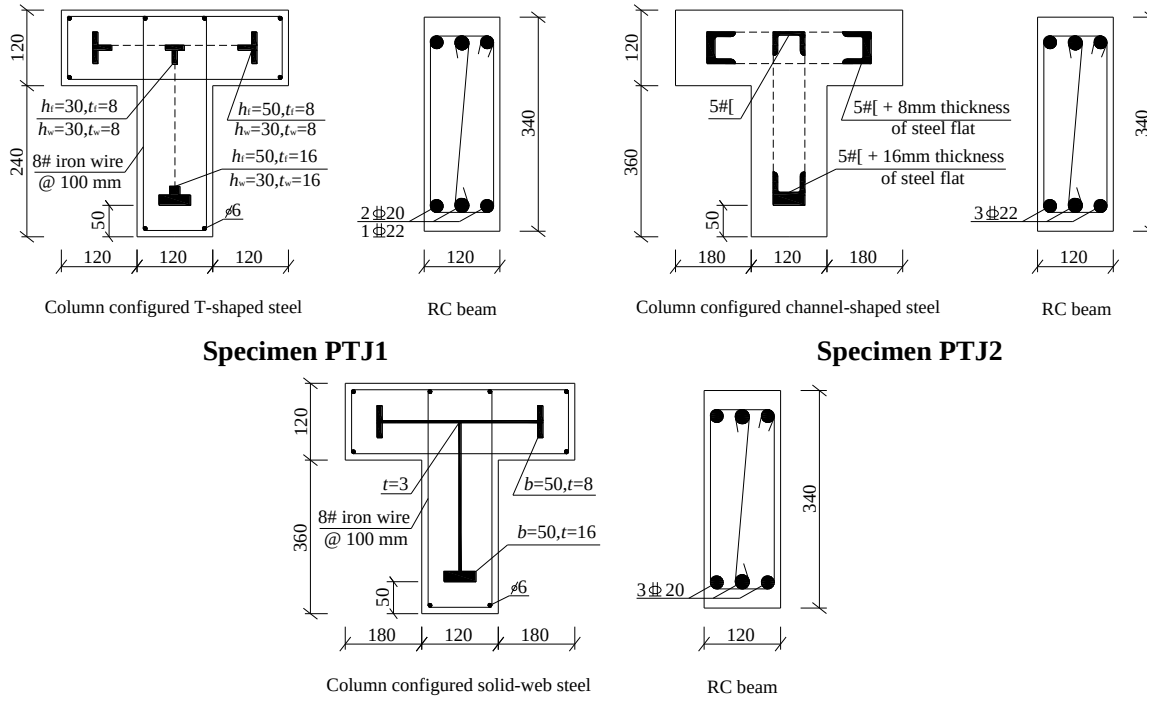

Fig. 1 Detailed parameters of cross sections for 2D joints

2.3 Test setup and loading sequences

The testing system shown in Fig. 4 consisted of a 250 kN servo-controlled hydraulic actuator to generate the cyclic horizontal load and a 500 kN hydraulic jack to apply the constant vertical load. In the presence of the hinge connection, the top of the specimen could rotate freely and only the shear force and the axial force could be transferred to the specimen, thereby the free end boundary condition was satisfied. Both the horizontal actuator and the vertical jack were connected to the sliding devices at the top end without rotation and to the hinge connection at the bottom end with a one-way hinge support. To ensure a hinge end condition, the inflection points of the steel beams were locked with two steel bars fixed to two large steel beam devices up and down, respectively. In this case, the cyclic horizontal load and the constant vertical load could act on the specimen along the horizontal and vertical directions respectively during the entire test.

In the test, the vertical load was applied to the specimen and then maintained constant. Horizontal force was imposed using the force-control scheme repeated only once at each control point before the specimen yields, and then using the displacement-control scheme repeated three times at each control point after the specimen yield. For all the specimens, the deformation of the upper column end was measured by LVDT.

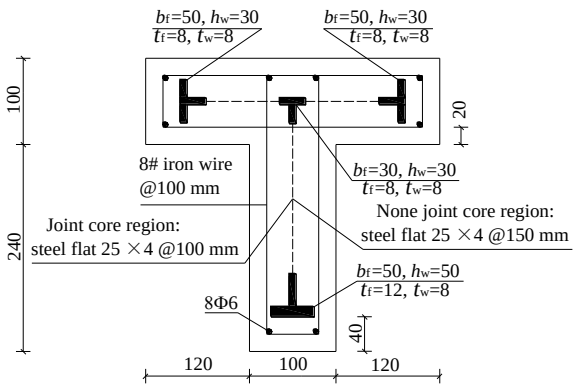

Columns configured T-shaped steel
(STJ3, STJ4)

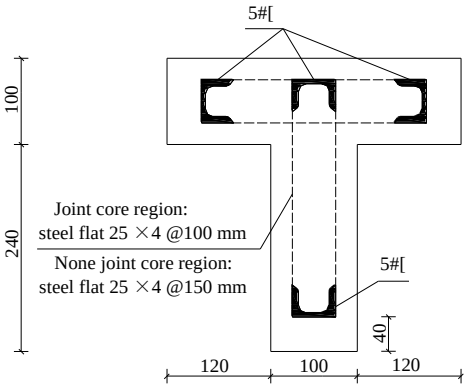

Columns configured channel-shaped steel
(STJ1, STJ5)

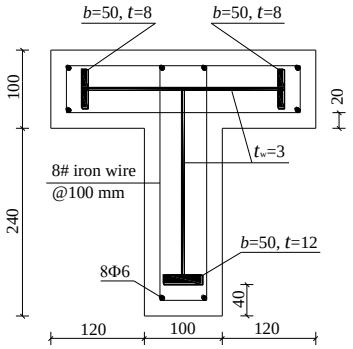

Columns configured solid-web steel
(STJ2, STJ6)

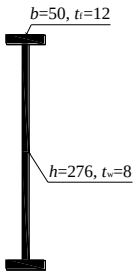

Steel beam

Fig. 2 Detailed parameters of cross sections for 3D joints

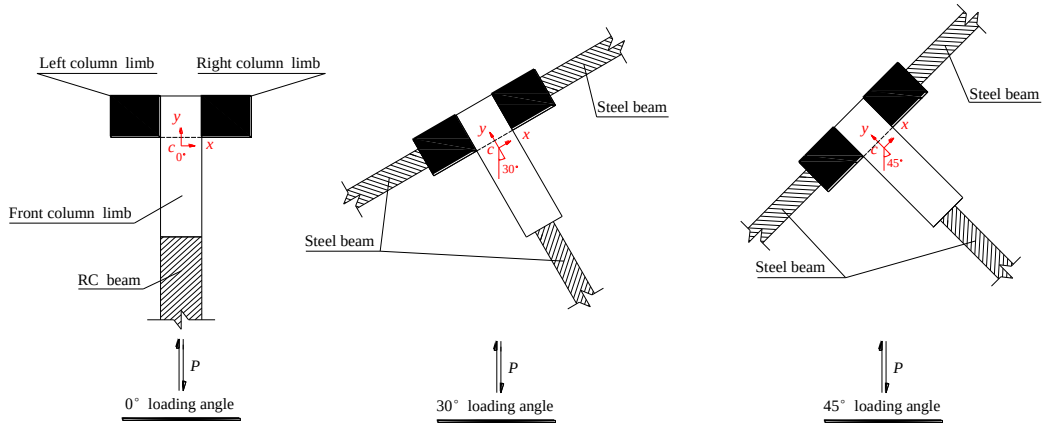

Fig. 3 Loading directions for specimens

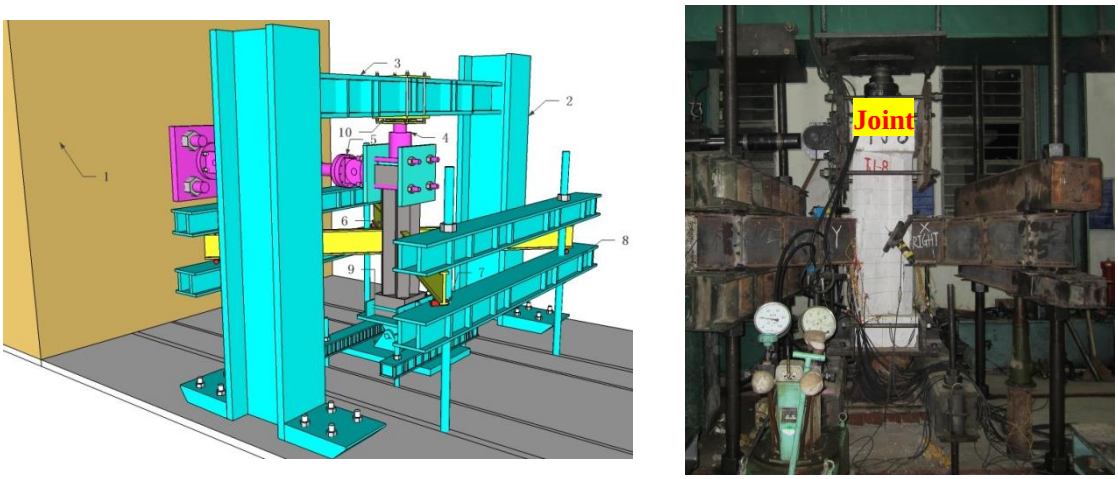

Note:
1 is the reaction wall; 2 is the counterforce frame; 3 is the counterforce beam; 4 is the hydraulic jack; 5 is the electro-hydraulic servo actuator; 6 is the specimen of 3D joint; 7 is the fixed steel bar; 8 is the device of steel beam; 9 is the one-way hinge support; 10 is the roller device.

Fig. 4 Test setup

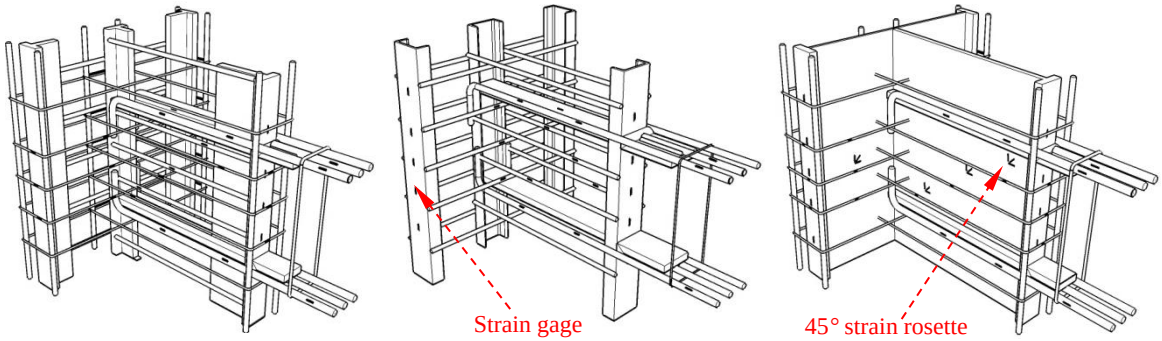

Fig. 5 Strain gages and 45° strain rosettes in the specimens

(a) 2D joints

(b) 3D joints

Fig. 6 Failure modes of specimens

In addition, the steel strain rosettes for the solid-web steel in the steel webs were arranged at the joint core to intensively investigate the development of shear deformation at the joint core, and some steel and steel reinforcement strain gages were also arranged at a critical beam-end section to monitor the beam-end flexural behavior as shown in Fig. 5.

3. Test results and discussion

3.1 Failure modes and cracking patterns

3.1.1 Planar joints

Since all the specimens of planar joints demonstrate the similar phenomenon in the tests, only the specimen PTJ1 is discussed here. In the load-control loading stage, when the lateral load reached positive 60 kN, large amounts of bending-shear diagonal cracks appeared at the concrete beam end near the column limb. Then the opposite loading to negative 60 kN resulted in densely

distributed bending-crossed shear diagonal cracks at the concrete beam end. After the specimen yield, multiple crossed diagonal cracks appeared on the T-shaped column limb connecting with the beam. In the displacement-control loading stage, these crossed diagonal cracks gradually divided the joint core surface into a number of diamond-shaped pieces. When the specimen nearly destroyed, the concrete on the front joint core column limb began to crush. In this test, it was worth noting that the existing of the left and right sides of column limbs (in Fig. 3) inhibited the fore crossed diagonal cracks through these limbs. After that, the area of the crushing concrete was gradually expanding with the increase of displacement amplitude. The final failure modes of all the 2D specimens are the shear diagonal-compression failure in the joint core and the failure pictures of the planar joints are illustrated in Fig. 6(a).

3.1.2 3D joints

Since all the specimens of 3D joints demonstrate the similar phenomenon in the tests, only the specimen STJ1 is discussed here. In the load-control loading stage, when the lateral load reached certain degree, multiple longitudinal bonding cracks appeared on the fore-and-aft surfaces of column limbs (perpendicular to the horizontal loading direction) along the concrete protective cover thickness of shape steel. After the specimen yield, large amounts of crossed shear diagonal cracks appeared at the joint core along the surfaces parallel to the horizontal loading direction. In the displacement-control loading stage, the concrete on the column limbs located at upper and lower flanges of the steel beams began to crush. After that, the crossed diagonal cracks gradually divided the joint core surface into a number of diamond-shaped pieces, and the core concrete at these regions also started to crush. The final failure modes of all the 3D specimens are the shear diagonal-compression failure with bonding cracks in the joint core, and the failure pictures of the 3D joints are illustrated in Fig. 6(b).

3.2 Hysteretic responses and normalized load-displacement curves

The load-displacement hysteretic curves of all the specimens are shown in Fig. 7. Here, contrasting the hysteretic loops of two kinds of specimens is an advisable way to explore the differences of seismic damage evolution and performance degradation between planar joints and 3D joints. Hence, the normalized method for hysteretic curves by eliminating the influences of experimental parameters such as cross section size of special shaped column, column length, concrete strength and size effect of the beam can achieve the before-mentioned requirements. The following process is described to carry out the normalized method for all the specimens.

(1) The cross section size of special shaped column and concrete strength class of the specimen are the critical factors to affect the shear bearing capacity of joint core. After normalized, the vertical coordinate load P (Unit: kN) is converted to $P\times10^3/f_c b_c h_0$, Where b_c is the cross section width of the column limb, $h_0=h-a_r$ is the effective height of the column limb cross section, h is the cross section height of the column limb, a_r is the thickness of concrete protective cover for longitudinal reinforcement or shape steel (if there is no longitudinal reinforcement outside the shape steel) corresponding to the direction of the above mentioned h. For the planar joint, the value of h_0 is the one which is in parallel to the direction of shear force; while for the 3D joint, the value of h_0 used is the maximum one in two directions of engineering axis.

(2) The interlayer displacement angle Δ/L_e defined in section 3.5 is one of the indexes to express the relative deformation ability of joint core. As Wu *et al*. (2010) suggested, this index can not only eliminate the influence of distance of L_e between upper inflection point and bottom

inflection point, but also can remove the influence of cross section characteristics and size effect in the beam. As a consequence, the interlayer displacement angle can be deemed as the horizontal axis for normalized hysteretic curves in the coordinate system.

Fig. 8 shows the normalized hysteretic curves of all the specimens and groups them by loading angle, where group A (channel-shaped steel form for specimens) is composed of the specimens PTJ2, STJ1 and STJ5, group B (T-shaped steel form for specimens) is consist of the specimens PTJ1, STJ3 and STJ4, and group C (solid-web steel form for specimens) is made up of the specimens PTJ3, STJ2 and STJ6. The axial compressive ratios in each group in this investigation are rather close, so that to some extent, their effects on the shape of hysteretic loop can be neglected. Here, it can be seen that the hysteretic loops for the specimens configured with solid-web steel are much plumper than those for the specimens configured with channel-shaped steel and T-shaped steel. In addition, it can be found in group A and group B that the hysteretic curves of 3D joints are a little more pinched than those of the planar joints, indicating that when the T-shaped specimen column is configured with non-solid-web steels (T-shaped or channel-shaped steel), the seismic behavior for the planar joints is superior to that for the 3D joints; while for the group C (here T-shaped specimen columns are configured with solid-web steel), the hysteretic curves of 3D joints are slightly plumper than that of the planar joint, indicating that the seismic behavior for the 3D joints to some extent can keep well under seismic-induced action. As for the spatial loading angles, the hysteretic loops for the specimens under 45° are generally plumper than those for the specimens under 30°. It means that under the 45° direction of horizontal seismic action to the SRC T-shaped columns, the composite materials in the joint core can be stimulated better than other directions of horizontal seismic spatial action due the stress homogeneity in the T-shaped cross section. Furthermore, it should be pointed out that whether the planar joints or 3D joints, the curves of all the specimens in each group on the descent stage have a similar falling and their descent processes are not too fast, indicating that the decreasing of shear strength for SRC T-shaped column-beam hybrid joints is not too large.

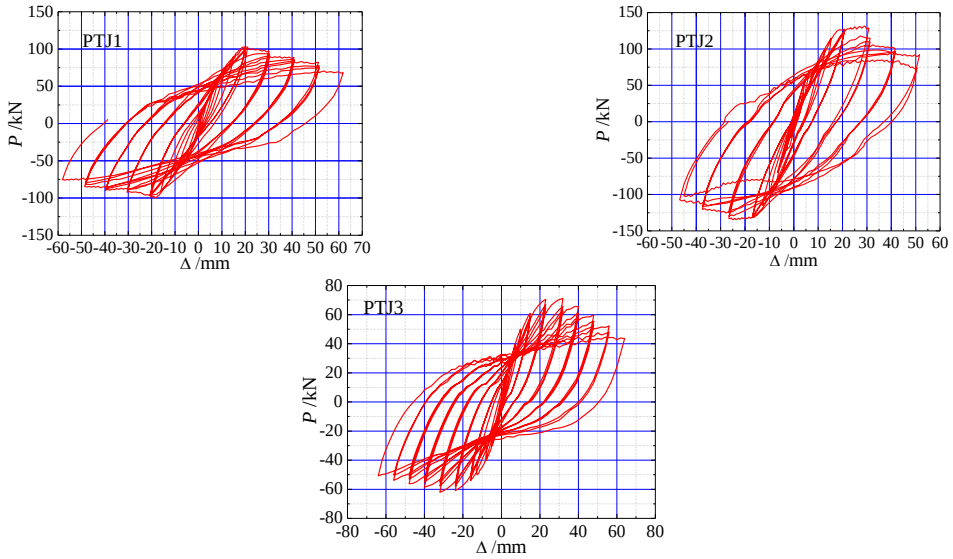

(a) Planar joints

Fig. 7 Hysteresis curves of specimens

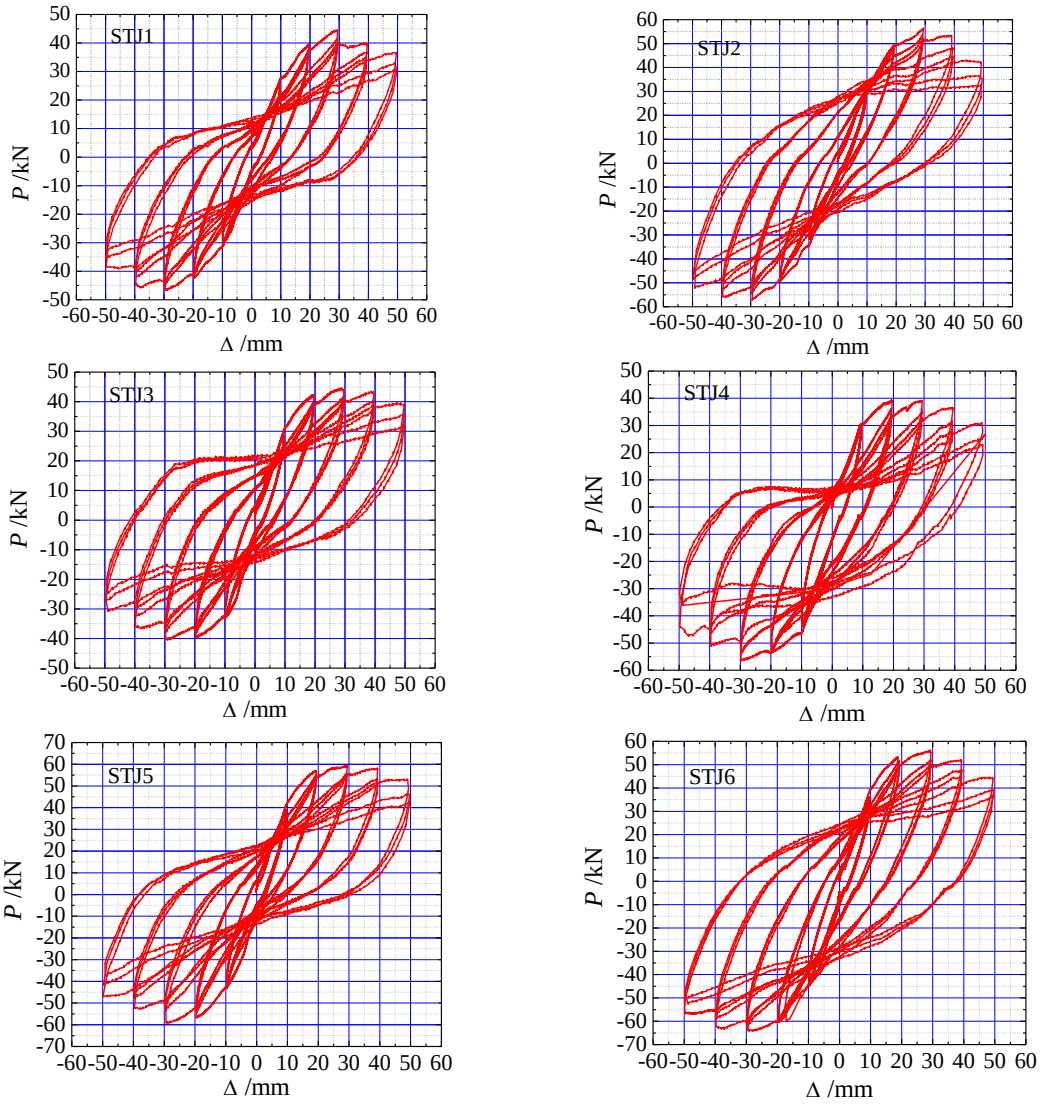

(b) 3D joints

Fig. 7 Continued

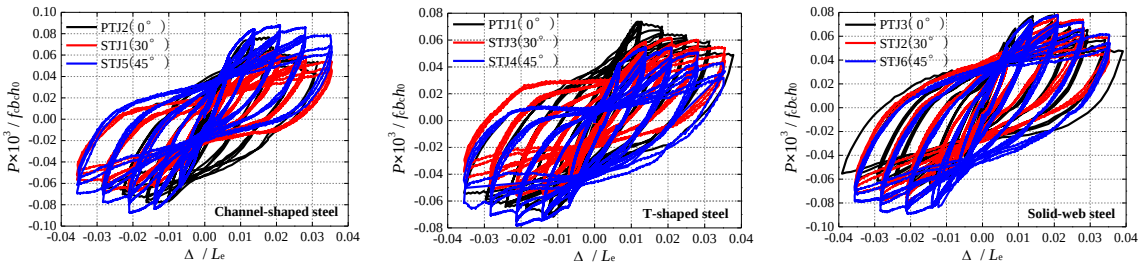

(a) Group A (b) Group B (c) Group C

Fig. 8 Normalized hysteresis curves

3.3 Energy dissipation capacity

In order to evaluate the accurate energy dissipation ability of all the specimens, the equivalent viscous damping ratio h_e is calculated by Eq. (1). $S_{(ABC+CDA)}$ and $S_{(OBE+ODF)}$ are the areas of the shadow as shown in Fig. 9. The curve is one of the cycles of hysteretic curve. The equivalent viscous damping ratios of all the hybrid joints are shown in Fig. 10.

$$h_e = \frac{1}{2\pi} \cdot \frac{S_{(ABC+CDA)}}{S_{(OBE+ODF)}} \tag{1}$$

The energy dissipation abilities between planar joints and 3D joints can be compared to explore the energy-dissipated mechanism as follows: (1) in group A, the h_e value of the specimen PTJ2 is averagely 22% larger than that of the specimens STJ1 and STJ5; (2) in group B, the h_e values of the specimens STJ3 and STJ4 are 4.08% and 2.38% larger than that of the specimen PTJ1, respectively; (3) compared to the specimen PTJ3, the equivalent viscous damping ratios of the specimens STJ2 and STJ6 in group C are increased by 1.95% and 17.58%, respectively. Overall, it can be seen that the equivalent viscous damping ratios of 3D hybrid joints are larger than those of the planar joints, indicating that the energy dissipation capacity of 3D hybrid joints is better than that of the planar hybrid joints. The reason is that the T-shaped 3D hybrid joint connected with three beams in the orthogonal directions leads to be a more complex stress state for the joint core, so that its failures such as the damage of steel and concrete can be more sufficient in comparison of the planar hybrid joint subjected to only one beam in plane.

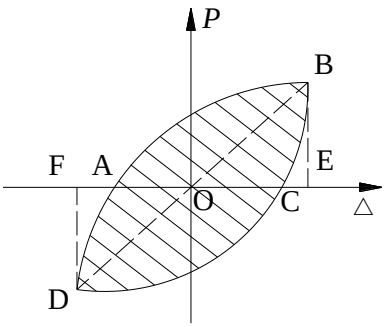

Fig. 9 Calculation model of equivalent viscous damping coefficient

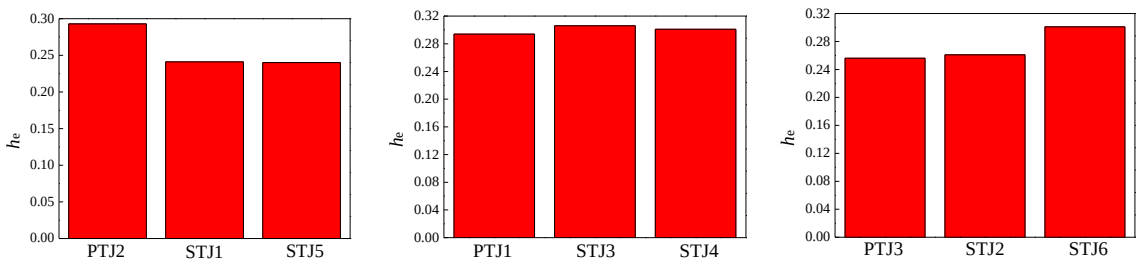

(a) Group A (b) Group B (c) Group C

Fig. 10 Comparison of equivalent viscous damping ratios between planar joints and 3D joints

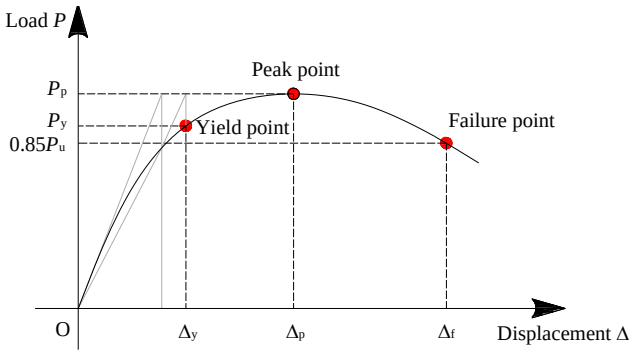

Fig. 11 Characteristic points on load–displacement curve

In addition, it can be clearly observed that both the energy dissipation abilities of the specimens PTJ1 (h_e=0.294) and PTJ2 (h_e=0.293) are better than that of the specimen PTJ3 (h_e=0.256) even if the cross-sectional steel ratio of the specimen PTJ3 is much larger than that of the specimen PTJ1 or PTJ2, which means that high cross-sectional steel ratio may not play a vital role in enhancing the energy dissipation ability for SRC T-shaped column-beam planar hybrid joints. On the contrary, a trend can be found that an increase of cross-sectional steel ratio leads to an increase of h_e for SRC T-shaped column-beam 3D hybrid joints, indicating that more shape steels are working together to resist to the external forces, so that the damage is more serious in the 3D joint core.

3.4 Ductility

Ductility plays a critical role in the seismic design of SRC structures. The displacement ductility ratio can be expressed as $\mu=\Delta_f/\Delta_y$, where Δ_f is the failure displacement corresponding to 85% of the ultimate load in the post-ultimate region of the skeleton curve; Δ_y is the yield displacement, and here the yield point (P_y, Δ_y) can be determined using the graphical method in Ref. (Nie *et al.* 2008) as shown in Fig. 11. The displacement ductility ratios of all the specimens are illustrated in Fig. 12, where μ is the mean result of positive value and negative value. It can be seen that the displacement ductility ratios of 3D hybrid joints in each group are almost close to those of the planar hybrid joints, indicating that the deformation performance of 3D hybrid joints is not worse than that of the planar hybrid joints. Additionally, it should be pointed out that the displacement ductility ratios vary from about 2.5 to 4.5, indicating that all the specimens feature certain but limited plastic deformation capacities. Thus, the potential possibility for SRC T-shaped column-beam hybrid joints being used in seismic zones beyond their elastic state is confirmed.

3.5 Interlayer displacement angle

Deformation capacity between the layers is one of the most significant indexes to evaluate the seismic performance of a structure. The interlayer displacement angle θ can be calculated as the ratio of horizontal displacement Δ to the distance between the inflection points of upper and lower columns (L_1+L_2), and its schematic diagrams for T-shaped 3D joints is shown in Fig. 13. Under the stipulation of current Chinese seismic code (GB 50011-2010) (2010), the elastic limit $[\theta]_e$ and inelastic limit $[\theta]_p$ for RC frame structures are 1/550 and 1/50, respectively. Table 2 lists the

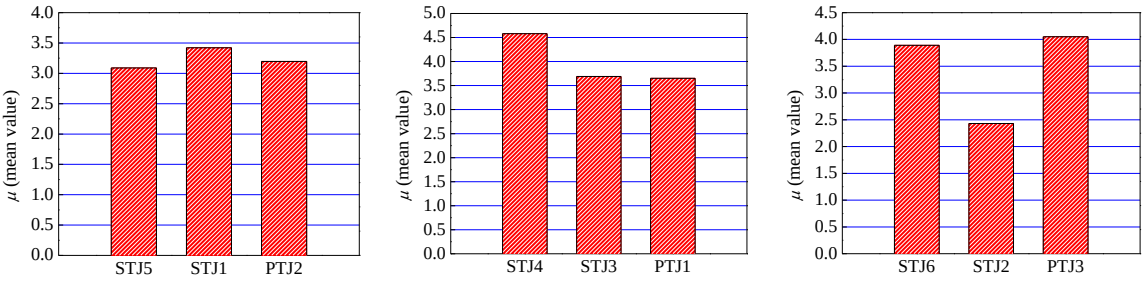

(a) Group A (b) Group B (c) Group C

Fig. 12 Comparison of displacement ductility ratios between planar joints and 3D joints

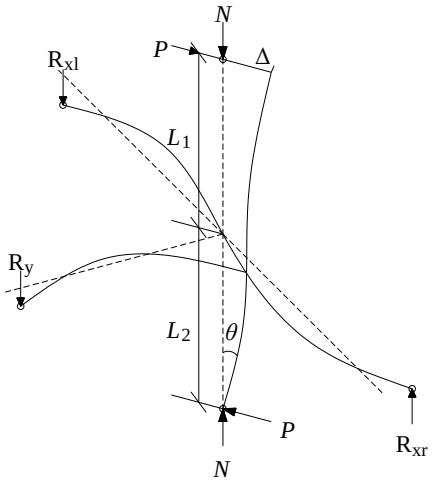

Fig. 13 Mode of interlayer displacement angle

characteristic interlayer displacement angles of all the specimens. It can be draw conclusions from Table 2 as follows:

(1) When the specimens yield, the θ_y of SRC T-shaped column-RC beam planar hybrid joints is 3.29-4.40 times $[\theta]_e$; while for the SRC T-shaped column-steel beam 3D hybrid joints, the θ_y values are 3.99-7.86 times $[\theta]_e$ for the specimens under 30° loading angle, and 3.37-5.91 times $[\theta]_e$ for the specimens under 45° loading angle. In view of this, it can be seen that the elastic interlayer deformation capacities between planar and 3D joints are close to each other, and their values are larger than the demand in the elastic deformation stage.

(2) When the specimens were destroyed, the θ_f of SRC T-shaped column-RC beam planar hybrid joints is 1.16-1.79 times $[\theta]_p$; while for the SRC T-shaped column-steel beam 3D hybrid joints, the θ_f values are 1.39-1.79 times $[\theta]_p$ for the specimens under 30° loading angle, and 1.52-1.79 times $[\theta]_p$ for the specimens under 45° loading angle. As a result, it can be obviously seen that the inelastic interlayer deformation capacity of the specimens grows with the increasing of loading angle (here from 0° to 45°), and the interlayer displacement angles of 3D joints in the failure point are all larger than the code requirement, indicating that its anti-collapse ability is good enough.

Table 2 Interlayer displacement angle for all the specimens

Group number		A			B			C		
Specimen code		PTJ2	STJ1	STJ5	PTJ1	STJ3	STJ4	PTJ3	STJ2	STJ6
θ_y	Positive	1/125	1/96	1/93	1/125	1/100	1/125	1/125	1/70	1/109
	Negative	1/167	1/110	1/98	1/142	1/138	1/163	1/125	1/74	1/121
θ_p	Positive	1/57	1/48	1/41	1/78	1/45	1/59	1/51	1/46	1/50
	Negative	1/65	1/45	1/49	1/89	1/53	1/49	1/51	1/45	1/42
θ_f	Positive	1/43	1/32	1/29	1/38	1/28	1/31	1/34	1/31	1/31
	Negative	1/38	1/29	1/33	1/34	1/36	1/31	1/28	1/28	1/28

Note: θ_p is the interlayer displacement angle of a hybrid joint when its load reaches the peak point.

3.6 Cumulative seismic damage

It is now generally accepted that the two-parameter model has a global effect on the level of the structural damage. Experiments on structural members and structures indicate that both the excessive deformation and hysteretic energy are the most important factors contributing to the seismic damage. Therefore, the damage models combining the deformation ductility and the hysteretic energy appear to be more reasonable for damage evaluation. Due to the large amount of test component samples in getting the Park-Ang model, there is no doubt that its reliability can be much better than other damage models to evaluate the structural seismic damage (Park *et al*. 1985). In this paper, the Park-Ang damage model is selected to reveal the influences of steel configuration type and loading angle on the damage of specimens.

$$D_{\text{P-A}} = \frac{\delta_{\text{m}}}{\delta_{\text{u}}} + \beta \frac{d\int E}{P_{\text{y}} \cdot \delta_{\text{u}}} \tag{2}$$

Where δ_m is the maximum deformation of member or structure under earthquake action; δ_u is the ultimate displacement under the monotonic loading, where it is determined from the skeleton curve; P_y is the yield load; $d\int E$ is the cumulative hysteretic energy and β is the energy parameter. However, the formula of β in the original literatures is obtained from the RC structure members, so that it is not suitable for applying to the SRC structures. In order to expand the scope of Park-Ang model in SRC structures, Liu *et al*. (2010) proposed the following equation by considering the parameters such as the steel ratio in the cross section ρ_{ss}, the shear-span ratio λ and the stirrup ratio ρ_{sv}.

$$\beta = -0.002\rho_{\text{ss}} + 0.005\lambda + 0.01\rho_{\text{sv}} \tag{3}$$

For comparison, the earthquake damage index D is determined as follows

$$D = \frac{D_{\text{P-A}}}{D_{\text{P-A,f}}} \tag{4}$$

Where $D_{P\text{-}A,f}$ is the damage function value when a structure is in the failure point. If D=0, there is no damage, and it means that the structure is in a state of safety; if D=1, the damage increases to the ultimate state, so that it can be considered that the structure is completely destroyed; If $D \in (0,1)$, the structure is in a state between absolute safety and destruction.

Fig. 14 shows the effect of steel configuration type on the cumulative damage of specimens. It can be seen that the damage accumulation for the specimens configured with T-shaped steel under the same condition of cumulative deformation is slightly larger than that for the specimens with channel-shaped and solid-web steels, indicating that the seismic-induced destruction of SRC T-shaped column-beam hybrid joint configured with T-shaped steel is more serious than that of the hybrid joints configured with other steel forms. In addition, the effect of loading angle on the cumulative damage of specimens is illustrated in Fig. 15. It can be observed that the rate of damage development for the planar joint is faster than that for the 3D joints; however, under the same condition of cumulative deformation and shape steel type, the damage accumulation for the specimen PTJ2 is rather close to that for the specimens STJ1 and STJ5. what's more, it can be found that the damage accumulation for the specimens subjected to 30° loading angle under the same condition of cumulative deformation is much larger than that for the specimens subjected to 45° loading angle, indicating that the stress uniformity under 45° is conducive to play the fullest role of each part of materials in the joint core.

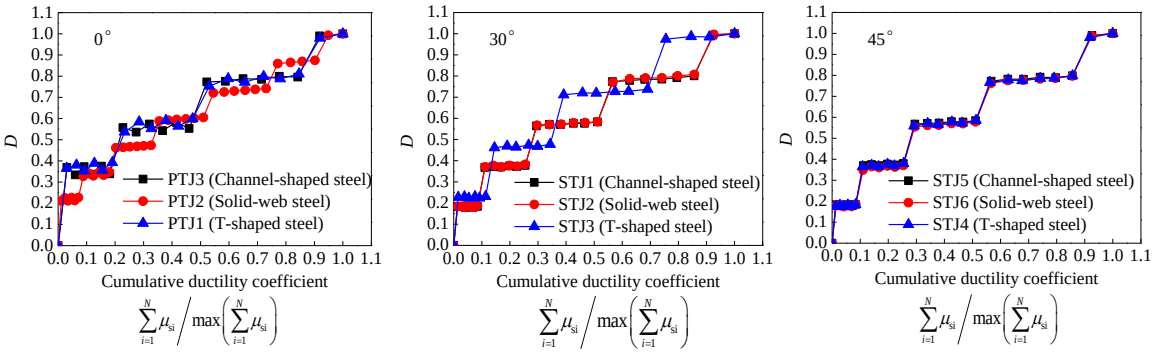

(a) 0° loading angle (b) 30° loading angle (c) 45° loading angle

Fig. 14 Effect of steel configured type on the cumulative damage of specimens

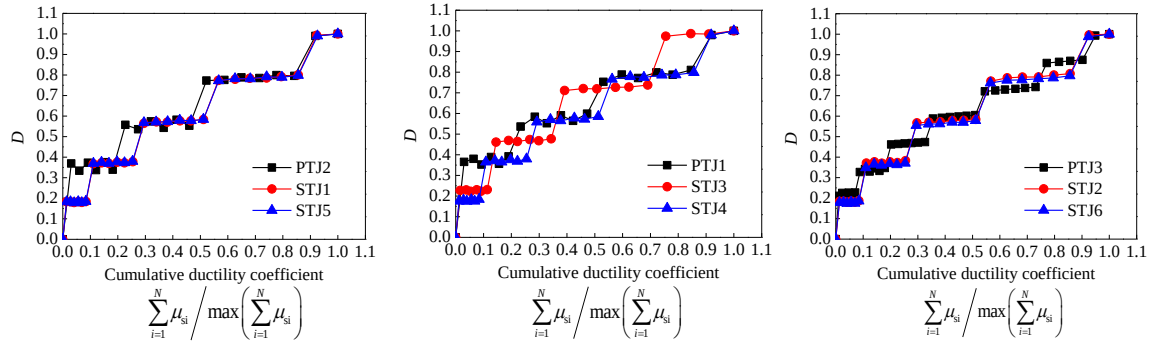

(a) Group A (b) Group B (c) Group C

Fig. 15 Effect of loading angle on the cumulative damage of specimens

4. Conclusions

This paper presents an experimental study on the seismic behavior of steel reinforced concrete T-shaped column-beam hybrid joints, including three planar joints and six 3D joints. From the investigation, the following conclusions are obtained:

(1) The test phenomenon shows that the shear-diagonal compressive failure is the dominating failure mode for all the specimens. In addition, for the planar hybrid joints, there is a suppressive effect of two sides of column limbs vertical to the loading direction on the penetration of oblique cracks; while for the 3D hybrid joints, bonding cracks are the auxiliary failure in the joint core.

(2) The hysteretic loops of the specimens configured with solid-web steel are much plumper than those of the specimens configured with channel-shaped steel and T-shaped steel. In addition, the hysteretic curves of 3D joints are a little more pinched than those of the planar joints, indicating that when the T-shaped specimen column is configured with T-shaped or channel-shaped steels, the seismic behavior for the planar joints is superior to that for the 3D joints; while for the specimen columns configured with solid-web steel, the hysteretic curves for 3D joints are slightly plumper than that of the planar joint, indicating that the seismic behavior for the 3D joints to some extent can keep well under seismic-induced action. Furthermore, the hysteretic loops for the specimens under 45° loading angle are generally plumper than those for the specimens under 30° loading angle.

(3) Overall, the equivalent viscous damping ratios of 3D hybrid joints are larger than those of the planar joints, indicating that the energy dissipation capacity of 3D hybrid joints is better than that of the planar hybrid joints.

(4) The displacement ductility ratios of 3D hybrid joints are almost close to those of the planar hybrid joints, indicating that the deformation performance of 3D hybrid joints is not worse than that of the planar hybrid joints.

(5) For the yielding point, the elastic interlayer deformation capacities between planar and 3D joints are close to each other, and their values are over the demand in elastic deformation stage evaluated by Chinese seismic code. While for the failure point, an increase of loading angle (from 0° to 45°) leads to an increase of inelastic interlayer deformation capacity of the specimens, and the interlayer displacement angles of 3D joints in the failure point are all larger than the code requirement.

(6) Under the same condition of cumulative deformation, the damage accumulation for the specimens configured with T-shaped steel is larger than that for the specimens with channel-shaped and solid-web steels, and the damage accumulation for the specimens subjected to 30° loading angle is much larger than that for the specimens subjected to 45° loading angle. As for the rate of damage development, the planar joint's is faster than that for the 3D joints.

Acknowledgements

The authors would like to thank the Natural Science Foundation of China (No. 50908057 and 51268004), the Open Project of Guangxi Key Laboratory of Disaster Prevention and Structural Safety (No: 2012ZDX10) and Innovation Project of Guangxi graduate education (No: YCBZ2012005). The founding and support from the above projects are greatly acknowledged.

References

Zhou, T., Chen, Z.H. and Liu, H.B. (2012), "Seismic behavior of special shaped column composed of concrete filled steel tubes", *J. Construct. Steel Res.*, **75**(8), 131-141.

Wu, B. and Xu, Y.Y. (2009), "Behavior of axially-and-rotationally restrained concrete columns with '+'-shaped cross section and subjected to fire", *Fire Safety J.*, **44**(2), 212-218.

Xu, Y.Y. and Wu, B. (2009), "Fire resistance of reinforced concrete columns with L-, T-, and +-shaped cross-sections", *Fire Safety J.*, **44**(2), 869-880.

Patton, M.L. and Singh, K.D. (2012), "Numerical modeling of lean duplex stainless steel hollow columns of square, L-, T-, and +-shaped cross sections under pure axial compression", *Thin Wall. Struct.*, **53**(4), 1-8.

Ramamurthy, L.N. and Hafeez, Khan, T.A. (1983), "L-shaped column design for biaxial eccentricity", *J. Struct. Eng*., ASCE, **109**(8), 1903-1917.

Marin, J. (1979), "Design aids for L-shaped reinforced concrete columns", *ACI J. Proc.*, **76**(11), 1197-1216.

Cheng-Tzu, T.W. (1985), "Biaxially loaded L-shaped reinforced concrete columns", *J. Struct. Eng*., ASCE, **111**(12), 2576-2595.

Hsu, T.C. (1989), "T-shaped reinforced concrete members under biaxial bending and axial compression", *ACI Struct. J.*, **86**(4), 460-468.

Mallikarjuna. and Mahadevappa, P. (1992), "Computer aided analysis of reinforced concrete columns subjected to axial compression and bending-I L-shaped sections", *Comput. Struct.*, **44**(5), 1121-1138.

Tsao, W.H., and Hsu, C.T.T. (1993), "A nonlinear computer analysis of biaxially loaded L-shaped slender reinforced concrete columns", *Comput. Struct.*, **49**(4), 579-588.

Dundar, C. and Sahin, B. (1993), "Arbitrarily shaped reinforced concrete members subjected to biaxial bending and axial load", *Comput. Struct.*, **49**(4), 643-662.

Yau, C.Y., Chan, S.L. and So, A.K.W. (1993), "Biaxial bending design of arbitrarily shaped reinforced concrete columns", *ACI Struct. J.*, **90**(3), 269-278.

Sinha, S.N. (1996), "Design of cross (+) section of column", *Indi. Concrete J.*, **70**(3), 153-158.

Kang, G.Y. and Gong, C.J. (1997), "Shear properties of T and L-shaped section frame columns under monotonic and horizontal low cyclic loadings", *J. Build. Struct.*, **18**(5), 22-31. (in Chinese)

Li, J., Wu, J.Y. and Zhou, D.Y. (2002), "Experimental research on wide flange specially shaped section columns subjected to cyclic loading", *J. Build. Struct.*, **23**(1), 9-14. (in Chinese)

Zhao, Y.J., Li, Z.X. and Chen, Y.X. (2004), "Research on limit values of axial compression ratios of specially shaped RC columns in case of 4th aseismic grade", *J. Build. Struct.*, **25**(3), 58-62. (in Chinese)

Cao, W.L., Huang, X.M. and Song, W.Y. (2005), "Experiment and non-linear element analyses of seismic behavior of short specially shaped columns with crossed reinforcing bars", *J. Build. Struct.*, **26**(3), 30-37. (in Chinese)

Xue, J.Y., Chen, Z.P. and Zhao, H.T. (2012), "Shear mechanism and bearing capacity calculation on steel reinforced concrete special-shaped columns", *Steel Compos. Struct.*, **13**(5), 473-487.

Zuo, Z.L., Cai, J. and Yang, C. (2012), "Eccentric load behavior of L-shaped CFT stub columns with binding bars", *J. Construct. Steel Res.*, **72**(5), 105-118.

Zuo, Z.L., Cai, J. and Yang, C. (2012), "Axial load behavior of L-shaped CFT stub columns with binding bars", *Eng. Struct.*, **37**(4), 88-98.

Wang, Q.T. and Chang, X. (2013), "Analysis of concrete-filled steel tubular columns with "\T\" shaped cross section (CFTTS)", *Steel Compos. Struct.*, **15**(1), 41-55.

Tokgoz, S. and Dundar, C. (2012), "Tests of eccentrically loaded L-shaped section steel fibre high strength reinforced concrete and composite columns", *Eng. Struct.*, **38**(5), 134-141.

Li, B. and Kulkarni, S.A. (2010), "Seismic behaviour of reinforced concrete exterior wide beam-column joints", *J. Struct. Eng*., ASCE, **136**(1), 26-36.

Li, B. and Chua, G.H.Y. (2009), "Seismic performance of strengthened reinforced concrete beam-column joints using FRP composites", *J. Struct. Eng*., ASCE, **135**(10), 1177-1190.

Yap, S.L. and Li, B. (2011), "Experimental investigation of RC exterior beam-column sub-assemblages for

progressive collapse", *ACI Struct. J.*, **108**(5), 542-552.
Kai, Q. and Li, B. (2012), "Experimental and analytical assessment on RC interior beam-column subassemblages for progressive collapse", *J. Perform. Constr. Fac.*, **26**(5), 576-589.
Pham, T.P. and Li, B. (2013), "Seismic behaviour of RC columns with light transverse reinforcement under different loading directions", *ACI Struct. J.*, **110**(5), 833-844.
Wu, T., Liu, B.Q. and Xing, G.H. (2010), *Seismic behavior of reinforced concrete frame joints with different depth beams*, Science Press, Beijing, China.
Nie, J.G., Qin, K. and Cai, C.S. (2008), "Seismic behavior of connections composed of CFSSTCs and steel-concrete composite beams: finite element analysis", *J. Constr. Steel Res.*, **64**(6), 680-688.
GB50011-2010 (2010), *Code for seismic design of buildings*, China Architecture and Building Press, Beijing, China.
Park, Y.J. and Ang. H.S. (1985), "Mechanistic seismic damage model for reinforced concrete", *J. Struct. Eng*., ASCE, **111**(4), 722-739.
Liu, Y., Guo, Z.X. and Huang, Q.X. (2010), "Experimental study of damage model for SRC columns", *J. Wuhan University of Technology*, **32**(9), 203-207. (in Chinese)

IT